Journal of Controlled Release 372 (2024) 295–303

Contents lists available at ScienceDirect

Journal of Controlled Release

journal homepage: www.elsevier.com/locate/jconrel

Ionizable nanoemulsions for RNA delivery into the central nervous system – importance of diffusivity

Mireya L. Borrajo [a,b,c], Aloia Quijano [a,c], Philipp Lapuhs [a,b,c], Ana I. Rodriguez-Perez [a,c,d], Shubaash Anthiya [a,b,c], José L. Labandeira-Garcia [a,c,d], Rita Valenzuela [a,c,d,*], María José Alonso [a,b,c,*]

[a] Center for Research in Molecular Medicine and Chronic Diseases (CiMUS), Av. Barcelona s/n, Campus Vida, University de Santiago de Compostela, 15782 Santiago de Compostela, Spain
[b] Department of Pharmacy and Pharmaceutical Technology, School of Pharmacy, University of Santiago de Compostela, 15782 Santiago de Compostela, Spain
[c] IDIS Research Institute, University of Santiago de Compostela, 15782 Santiago de Compostela, Spain
[d] Networking Research Center of Neurodegenerative Diseases (CIBERNED), Madrid, Spain

ARTICLE INFO

Keywords:
Brain delivery
Diffusivity
mRNA
Nanoemulsion
RNA therapeutics
siRNA

ABSTRACT

Lipid nanoparticles (LNPs) currently dominate the RNA delivery landscape; however their limited diffusivity hampers targeted tissue dissemination, and, hence, their capacity for intracellular drug delivery. This is especially relevant for tissues such as the central nervous system (CNS), where overcoming proactive brain barriers is crucial for the efficacy of genetic therapeutics. This research aimed to create ionizable nanoemulsions (iNEs), a new generation of RNA delivery systems with enhanced diffusivity. The developed iNEs (consisting of the combination of C12–200, DOPE, Vitamin E, and DMG-PEG) with a size below 100 nm, neutral surface charge, and high RNA loading capacity, showed excellent cell viability and transfection efficiency in various cellular models, including neurons, astrocytes, and microglia. Subsequently, iNEs containing mRNA GFP were tested for CNS transfection, highlighting their exceptional diffusivity and selective transfection of neurons following intraparenchymal administration.

1. Introduction

Currently, the potential of RNA therapeutics for treating multiple medical conditions heavily relies on nanotechnology. Among nanocarriers, lipid nanoparticles (LNPs) are the sole market-approved delivery system for messenger RNA (mRNA) and small interfering RNA (siRNA) delivery [1]. The first LNP-based genetic therapeutic, Onpattro® (Alnylam), was approved in 2018 for the treatment of hereditary transthyretin-mediated amyloidosis [2]. In late 2020, mRNA vaccines, Comirnaty® (BioNTech/Pfizer) and Spikevax® (Moderna), were approved against the severe acute respiratory syndrome coronavirus 2 (SARS-CoV-2), the cause of the coronavirus disease 2019 (COVID-19) pandemic [3].

In these formulations, LNPs encapsulate mRNA with components including an ionizable lipid, cholesterol, a helper lipid, and a PEGylated lipid [4]. Ionizable lipids are responsible for the complexation of the RNA. They possess the ability to transition from neutral to positively charged in acidic endosomal pH, promoting fusion with the endosomal membrane and cargo release in the cytoplasm of the targeted cells [5–7]. While the unsaturated ionizable lipid DLin-MC3-DMA was used in Onpattro®, further optimization introduced multi-tail ionizable lipids in the research field, such as C12–200, enhancing endosome disruption [8–10]. Unfortunately, the degradability of these ionizable lipids remains a limitation, mainly due to their stable backbones [11]. Recent advances in the field focus their efforts on the development of the next generation of ionizable lipids, aiming to enhance their transfection performance while improving their biodegradability, ensuring their overall safety and low toxicity profile [12–14].

When designing a nanocarrier, successful *in vivo* transfection is not the sole requirement for nanocarrier design. After administration, the nanocarrier must reach the intended tissue, diffuse across it, and effectively reach the targeted cell. The limited diffusion of LNPs in the central

* Corresponding authors at: Center for Research in Molecular Medicine and Chronic Diseases (CiMUS), Av. Barcelona s/n, Campus Vida, University de Santiago de Compostela, 15782 Santiago de Compostela, Spain.
E-mail addresses: rita.valenzuela@usc.es (R. Valenzuela), mariaj.alonso@usc.es (M.J. Alonso).

https://doi.org/10.1016/j.jconrel.2024.06.051
Received 14 May 2024; Accepted 20 June 2024
Available online 24 June 2024

nervous system (CNS) has been extensively noted. For example, studies on LNP diffusion in the brain revealed reduced PTEN (phosphatase and tensin homolog-1) levels in neurons within 1 mm after the administration of LNPs containing PTEN-siRNA [15]. This was corroborated by Cy5-labeled mRNA LNPs administered in the striatum, detecting signals 1–1.5 mm from the injection site [16]. Unfortunately, the majority of studies quantifying nucleic acids in the brain do not provide information about their specific localization across the tissue [17,18].

The hypothesis of this work was that the limited diffusivity of LNPs across the brain may stem from their dense core and relative rigidity [19]. The same may apply to other solid-core nanoparticles [20,21]. Hence, our objective was centered on the development of softer, fluid, and deformable cores, such as in nanoemulsions (NEs). NEs, with nanometric droplet sizes, typically consist of an oil-in-water suspension of oils and surfactants [22,23]. Up until now, NEs have been extensively used for the solubilization of small hydrophobic molecules and some preliminary efforts have been oriented to accommodate RNA molecules [24]. For example, some authors have found that incorporating cationic lipids and surfactants into NEs allowed RNA absorption, and proposed their use in the field of mRNA vaccination [25–27]. In addition, cationic NEs containing 1,2-dioleoyl-3-trimethylammonium propane (DOTAP) were reported for the intranasal administration of siRNA anti-tumor necrosis factor-α (TNF-α), showing a positive reduction of anti-inflammatory markers in the brain. [28]. Similarly, a DOTAP-containing NE, intranasally delivered siRNA CD73 for glioblastoma treatment, significantly reduced tumor growth in an animal model [29]. However, none of these studies elucidated the role of deformability or particle composition of the positive results on successful drug delivery across the brain. Aligned with the soft and fluid core concept, studies indicate that both the particle size and internal composition of the nanocarriers can improve diffusion properties. For example, diffusivity studies in mucus and brain demonstrated that PEGylation of nanoparticles can enhance their diffusivity profile in a size-dependent manner [30–32].

Here, we leverage the knowledge of our lab in NEs and nanocapsules (NCs) delivery platforms to develop the next generation of ionizable NEs (iNEs) [33–39]. We explored various PEGylated lipid lengths for optimal transfection efficiency and low toxicity *in vitro*. Additionally, cytotoxicity profiles and transfection efficiency were assessed in neuronal, microglial, and astrocytic cellular models. To validate our hypothesis on enhanced diffusivity of iNEs, intra-parenchymal administration in rats using iNEs encapsulating GFP mRNA was performed. This aimed to elucidate specific CNS cells expressing GFP and the diffusivity profile of iNEs, for their possible application as gene delivery systems for the treatment of various CNS diseases.

2. Materials and methods

2.1. Materials

C12–200, HCl salt (1, 1′-((2-(4-(2-((2-(bis(2-hydroxydodecyl)amino) ethyl)(2-hydroxydodecyl)amino)ethyl)piperazin-1-yl)ethyl)azanediyl) bis(dodecan-2-ol)) and DMG-PEG_{2000} ((*R*)-methoxy-polyethyleneglycol-2000-carbamoyl-di-O-myristyl-sn-glyceride) were kindly gifted by Muthiah Manoharan, from Alnylam Pharmaceuticals (MA, USA). DOPE (1,2-dioleoyl-sn-glycerol-3-phosphoethanolamine) was purchased from Avanti Polar Lipids (AL, USA). Vitamin E (Vit E) (D, L-α-tocopherol) was obtained from BASF (Mannheim, Germany). siGFP (siRNA anti-GFP) was acquired from BioSpring GmbH (Frankfurt, Germany). mGFP (mRNA encoding for GFP, CleanCap EGFP mRNA) was purchased from TrikLink Biotechnologies (CA, USA).

2.2. Formulation of iNEs

iNEs were prepared in a single step, using a microfluidic mixer NanoAssemblr™ bench-top instrument, Precision NanoSystems Inc. (Vancouver, Canada), following a solvent displacement technique [40]. Formulation of the iNE and complexation of the oligonucleotide cargo occurred simultaneously. In summary, 0.2 mL of the organic phase (12.8 mg/mL of C12–200, 3.7 mg/mL of DOPE, 6 mg/mL of Vitamin E, and 2 mg/mL of DMG-PEG_{2000} in EtOH, leading to molar ratio of 35:16: 46.5: 2.5) were mixed with 1 mL of the aqueous phase (containing 0.24 mg/mL of the selected RNA diluted in citrate buffer, pH 4, 10 mM).

The nitrogen-to-phosphate ratio (between the amine groups of C12–200 and the phosphate groups of the RNA) was maintained at 15:1. The Flow Rate Ratio was 1:5 (organic to aqueous phase). The Total Flow Rate was maintained at 12 mL/min. The resulting iNE-RNA formulations presented a theoretical RNA concentration of 0.2 mg/mL. Samples were set aside for stabilization for 10 min before physicochemical characterization.

iNEs containing Tween 80® were prepared by bulk mixing, in a single step. Briefly, 0.2 mL of the organic phase (12.8 mg/mL of C12–200, 3.7 mg/mL of DOPE, 6 mg/mL of Vitamin E, and 1 mg/mL of Tween 80® in EtOH, leading to molar ratio of 35: 16: 46.5: 2.5) were added over 1 mL of the aqueous phase (containing 0.24 mg/mL of RNA diluted in citrate buffer 10 mM, pH 4). The aqueous phase was under stirring at 1400 rpm, and the resulting solution was kept under agitation for 5 s. Then, it was let to stabilize for 10 min before physicochemical characterization.

2.3. Physicochemical characterization of iNEs

The hydrodynamic diameter and polydisperse index (PDI) were characterized by dynamic light scattering (Zetasizer® Nano ZS, Malvern Instruments, Malvern, UK). ζ-potential was measured in terms of mean electrophoretic mobility values, measured by laser Doppler electrophoresis with the same equipment. Particle size and PDI measurements were performed after diluting the samples 10-fold in 1× PBS, pH 7. ζ-potential characterization was performed after dilution of samples 20-fold in RNase-free water.

Encapsulation efficiency (EE%) was determined following different methodologies. In all cases, iNE-RNA formulations were diluted in a 1:1 (*v*/v) ratio with Triton X-100 or heparin solutions, prepared at 50 mg/mL in RNase-free water. Incubation with Triton X-100 (Sigma-Aldrich, MO, USA) induced the disruption of the nanocarrier, while heparin (Sigma-Aldrich, MO, USA) led to the displacement of the RNA from the nanoparticle. Agarose gel electrophoresis was used to qualitatively assess the amount of RNA encapsulated in iNE-RNA formulations. Samples containing 1–3 μg of RNA were loaded in an agarose gel at 1% *w/v* in Tris Acetate-EDTA buffer (Sigma-Aldrich, MO, USA) before and after incubation with Triton X-100 and heparin. Samples were diluted with equal volumes of loading mix, containing 6× SYBR® Gold nucleic acid strain (Invitrogen, CA, USA), 44% Glycerol, and 0.176 g/L Bromophenol blue. Free RNA was included as a control. Gels were run for 30 min at 90 V in Sub-Cell GT cell 96/192 (Bio-Rad Laboratories, CA, USA), and evaluated with a UV transilluminator imaging system (Molecular Imager® Gel Doc™ XR, Bio-Rad Laboratories, CA, USA).

To quantitatively determine the EE% of iNE-RNA formulations, Quant-iT RiboGreen RNA assay kit (Invitrogen, MA, USA) was used. Briefly, samples were diluted 50-fold in TE buffer (1×), followed by a 2-fold dilution with Triton X-100 and incubation at 37 °C for 30 min. Subsequently, samples were diluted 10-fold with TE buffer (1×). The standard curve was prepared using RNA at concentrations between 0.1 and 1 μg/mL, in the presence of Triton X-100. Following manufacturer instructions, RiboGreen reagent was diluted 200-fold in TE buffer (1×), and added to an equal volume of sample, leading to a final volume of 200 μL. Samples and the standard curve were transferred to a 96-black polystyrene reader (Synergy H1, BioTek Instruments, VT, USA), using excitation at 485 nm and emission at 530 nm. The standard curve ($r^2 \geq 0.99$) was used for determining the RNA concentration of the sample. The encapsulation efficiency of RNA was calculated according to the following Eq. 1.

$$Encapsulation\ efficiency\ (EE\%) = \frac{Free\ or\ unencapsulated\ RNA}{Total\ RNA} \times 100$$

Where $[RNA]_{disrupted}$ is the RNA concentration determined after treating the nanosystems with the disrupting agent. $[RNA]_{theoretical}$ is the theoretical total RNA concentration of the nanosystem.

Equation 1 Calculation of encapsulation efficiency (EE%).

2.4. In vitro iNE-siGFP transfection efficiency and cytotoxicity in HeLa cells

Assessment of cytotoxicity and transfection efficiency was performed in HeLa cells expressing GFP, which were kindly gifted by Prof. Javier Montenegro (Center for Research in Biological Chemistry and Molecular Materials, CiQUS, Santiago de Compostela, Spain). A total of 10,000 cells were seeded per well in a flat bottom 96-well plate and allowed to adhere for 24 h. Cells were treated with iNE-siGFP for 4 h, in Opti-MEM™ (Gibco™, Thermo Fisher, MA, USA) at siGFP concentrations ranging from 250 to 10 nM per well. Nanocarriers were then removed and replaced with a complete medium (DMEM supplemented with 10% fetal bovine serum). Cells were incubated for another 20 h. Cell viability was measured by fluorescence-based resazurin assay [41]. Briefly, cells were incubated with resazurin reagent (Resazurin sodium salt, Sigma-Aldrich, MO, USA) supplemented complete media for 45 min, and the resulting fluorescence was measured in a plate reader at 544/590 nm. Cells were then trypsinized, harvested, and fixed with 1% (*w/v*) formaldehyde in PBS. The percentage of GFP-negative cells and mean fluorescence intensity (MFI) were analyzed by flow cytometery (BD Accuri, BD Biosciences, NJ, USA).

2.5. In vitro iNE-mGFP transfection efficiency and cytotoxicity in neuron, astrocyte, and microglia models

In vitro cytotoxicity and transfection efficiency were evaluated in human neuronal (SH-SY5Y cell line), rat astrocytic (C6 glioma cell line), and human microglial (CHME-3 cell line) models. For that, a total of 150,000 cells were seeded per well in a flat bottom 12-well plate and allowed to adhere for 24 h. Cells were treated with iNE-mGFP in Opti-MEM™ (Gibco™, Thermo Fisher, MA, USA) at a concentration of 5 μg per well, for 4 h. Nanocarriers were then removed and replaced with a complete medium. Cells were incubated for another 20 h. Cell viability was measured by absorbance-based MTT assay (3-(4, 5-dimethyl-2-thiazolyl)-2, 5-diphenyl-2H-tetrazolium bromide; Sigma-Aldrich, MO, USA). Briefly, cells were incubated with MTT reagent (1 mg/mL) for 4 h at 37 °C. After removing the MTT reagent, the resulting formazan crystals were dissolved in acidic isopropanol and quantified in a plate reader at 544/590 nm (Infinite 200 PRO, Tecan, Männedorf, Switzerland). For transfection efficiency assessment, cells were trypsinized, harvested, and fixed with 1% (*w/v*) formaldehyde in PBS. The percentage of GFP-positive cells and mean fluorescence intensity were analyzed by flow cytometry (BD Accuri, BD Biosciences, NJ, USA).

2.6. Animal studies

The animal study protocol was carried out following the European Communities Council Directive 2010/63/EU, Directive 86/609/EEC, and Spanish RD 526/2014, and was approved by the corresponding committee at the University of Santiago de Compostela (protocol 14,715,012/2021/012; last version 16 April 2021).

2.7. Assessment of diffusivity profile of iNE-mGFP upon intra-parenchymal administration

Administration of iNEs was performed in male Sprage-Dawley rats (3 animals in the iNE-mGFP group and 1 animal in the PBS, control group) deeply anesthetized with ketamine (50 mg/kg) and medetomidine (0.4 mg/kg). Anesthetized animals were mounted in a stereotaxic frame (Kopf Instruments, CA, USA) and were injected with 3 μg of mGFP encapsulated onto iNEs, in a total volume of 3 μL. The solution was injected using a 5- μL Hamilton syringe, coupled to a motorized injection (Stoelting), at a rate of 0.5 μL/min. Stereotaxic coordinates were A/P: 0.8 mm, M/L: 3.0 mm and D/V: 5.0 mm. The needle used for the administration was left in place for an additional 5 min before withdrawal to avoid iNEs reflux. After 24 h, animals received an anesthetic overdose and they were sacrificed by decapitation; their brains were rapidly removed, cryoprotected, and cut into coronal tissue sections using a sliding microtome. Sections were processed for immunofluorescence labeling as follows.

Free-floating tissue sections were pre-incubated in KPBS-1% BSA with 5% normal donkey serum (Sigma-Aldrich, MO, USA) and 0.03% Triton X-100 for 60 min at room temperature. Initially, single immunofluorescence was performed to identify cells capable of expressing GFP after mGFP transfection. The different brain cell types were labeled with primary antibodies against class III β-tubulin (β III-tubulin, 1:750, T8660, Sigma-Aldrich, MO, USA) as a neuronal maker, or glial fibrillary acidic protein (GFAP, 1:500, MAB360, Merk Millipore, MA, USA) as an astrocytic marker, or ionized calcium-binding adaptor molecule 1 (Iba-1, 1:500, 019–19,741, Wako Chemicals, Neuss, Germany) as a microglial maker. Cell nuclei were marked with the DNA-binding dye Hoechst 33342 (1:2000, 62,249, Sigma-Aldrich, MO, USA). Immunoreaction was visualized with the fluorescence secondary antibody Alexa Fluor 568-conjugated donkey anti-rabbit IgG (1:200, Molecular Probes, OR, USA) or Alexa Fluor 488-conjugated donkey anti-mouse IgG (1:200, Molecular Probes, OR, USA). Sections were mounted on gelatin-coated slides and cover-slipped with Immumount (Thermo-Shandon). Co-localization of these markers was assessed by confocal laser microscopy (AOBS-SP5X; Leica Microsystems Heidelberg GmbH, Mannheim, Germany).

Then, considering the auto-green fluorescence depicted by neurons [42], the decision was made to perform a double immunofluorescence against GFP (anti-GFP, 1:1000, C10362, Molecular Probes, OR, USA) and β III-tubulin, followed by the incubation with fluorescence secondary antibodies Alexa Fluor 568-conjugated donkey anti-rabbit IgG (1:200, Molecular Probes, OR, USA) and Alexa Fluor 488-conjugated donkey anti-mouse IgG (1:200, Molecular Probes, OR, USA), respectively. Then, the preparation of the section was performed as previously described.

3. Results and discussion

To maximize gene therapy effectiveness, nanocarriers must not only safeguard RNA cargo but also enable efficient diffusion across targeted tissues, especially in challenging tissues such as the CNS. For the design of nanosystems with enhanced diffusivity, we explored combining lipids, which are typical components of LNPs with oily cores from NEs for gene delivery in the CNS. The primary objective was to create a nanocarrier exhibiting extensive diffusion in the brain, ensuring effective delivery and transfection capacity with different types of RNA.

3.1. Development of ionizable nanoemulsions (iNEs)

To enhance brain diffusion, we designed a fluid NE with a Vitamin E core combined with the ionizable lipid C12–200 [43]. Known for its cone-shaped structure, C12–200 boosts endosomal disruption, crucial for efficient oligonucleotide release [10]. Upon cellular uptake, it becomes protonated in acidic endosomes, triggering a phase change that disrupts the endosomal membrane, facilitating cargo release into the cytosol [44]. The combination of an oily core with a lipid capable of enhancing endosomal escape holds promise for achieving effective brain diffusion and modulating CNS genes.

The initial screening of conditions involved bulk mixing, where

C12–200, DOPE, Vitamin E, and Tween 80® were combined at various molar ratios. This preliminary investigation led to the identification of a specific molar composition (35: 16: 46.5: 2.5) that allowed a relatively small particle size (165 nm, PDI 0.1) and a positive surface charge (+20 mV). Once this molar composition was fixed, increased N/P ratios (molar ratio of nitrogen atoms in the complexing lipid to phosphate atoms in the RNA) were explored, resulting in the identification of the full entrapment of the RNA at N/P ratio 15:1. The physicochemical properties of this initial formulation using different types of RNA can be found in Supplementary Table 1. Tween 80® was also substituted by DMG-PEG$_{2000}$, this being a more typical PEGylated material for RNA delivery.

Furthermore, the formulation process underwent adaptation for microfluidic preparation. The result was a notable reduction in particle size, which was attributed to the fine-tuning of mixing parameters (speed and shape of the convergence of both aqueous and organic phases within the device) [45,46]. Additionally, the presence of the DMG-PEG$_{2000}$ could also contribute to the reduction in size of the resulting iNE [45,47].

To showcase the versatility of the developed nanosystems, various types of RNAs were encapsulated into the iNEs. The physicochemical properties of the resulting iNEs, summarized in Table 1, indicate that, irrespective of the cargo, the particle diameter, PDI, or surface charge are very similar. This consistency illustrates the robustness of the iNE for delivering diverse oligonucleotide types.

The encapsulation efficiency and release behavior were assessed through agarose gel electrophoresis (Fig. 1), after dilution of the iNEs in different buffers (citrate buffer (CB) at pH 4, and phosphate buffer saline (PBS) at pH 7.4). C12–200 exhibits a positive charge at acidic pH, thus facilitating RNA condensation, and becomes neutral at physiological pH [48–50]. The results in Fig. 1 indicate that no free-RNA and hence no release was observed upon dilution at pH 4 (CB condition) regardless of the RNA type. At physiological pH (7.4, PBS condition), most RNA molecules remain complexed within the iNE, necessitating Triton X-100 disruption for complete release.

3.2. *In vitro assessment of iNEs with different PEGylated compounds in HeLa cells*

In vitro experiments were conducted using HeLa cells to assess the cytotoxicity and transfection efficiency of iNEs, employing siGFP as a model RNA molecule. A comparison was made between iNE formulations containing Tween 80® (prepared by bulk mixing) and DMG-PEG$_{2000}$ (prepared by microfluidic mixing).

Regarding cellular cytotoxicity (Fig. 2-A), iNE-DMG-PEG$_{2000}$ exhibited higher cell viability than iNE-Tween 80® at the highest concentrations (250 and 100 nM), displaying similar behavior at lower concentrations (50 and 10 nM). On the other hand, both iNE formulations showed comparable transfection efficiency (percentage of transfected cells and fluorescence intensity), and, thus, similar protein translation profiles at all concentrations tested (Fig. 2-B). However, it should be highlighted that at relatively low RNA concentrations (50 nM), the transfection efficiency and toxicity were similar for both types of formulations. Despite these relatively minor differences, the iNE containing DMG-PEG$_{2000}$, prepared by microfluidics, was selected for subsequent studies. Of note, the silencing effect was even observed at very low concentrations of siRNA.

Table 1
Physicochemical properties of iNE developed, containing C12–200, DOPE, Vitamin E, and DMG-PEG, in combination with siGFP and mGFP.

Typer of RNA	Size (nm)	PDI	ζ-Potential (mV)	Encapsulation efficiency (%)
siGFP	64 ± 7	0.23 ± 0.03	(−)2 ± 1	80–90
mGFP	72 ± 9	0.17 ± 0.07	(−)4 ± 2	80–90

Encapsulation efficiency was measured by agarose gel, and values were corroborated by RiboGreen assay. Abbreviations: GFP: green fluorescence protein. mGFP: mRNA encoding GFP. PDI: polydispersity index. siGFP: siRNA anti-GFP. Values represent the mean ± standard deviation ($n \geq 3$).

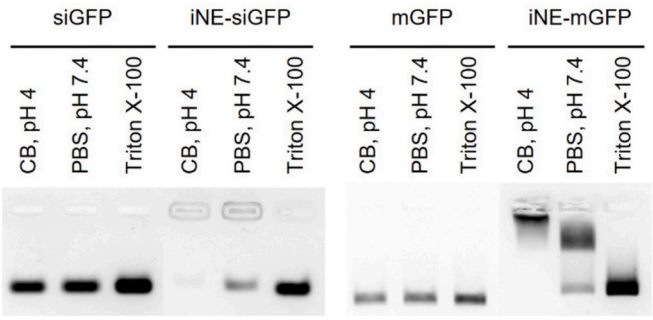

Fig. 1. Encapsulation efficiency of siGFP (left) and mGFP (right) loaded iNE. Samples were treated with CB (pH 4), PBS (pH 7.4), and Triton X-100 (for iNE disruption).
Abbreviations: CB: Citrate buffer. GFP: Green fluorescence protein. iNE: Ionizable nanoemulsion. mGFP: mRNA encoding GFP. PBS: Phosphate-buffered saline. siGFP: siRNA anti-GFP

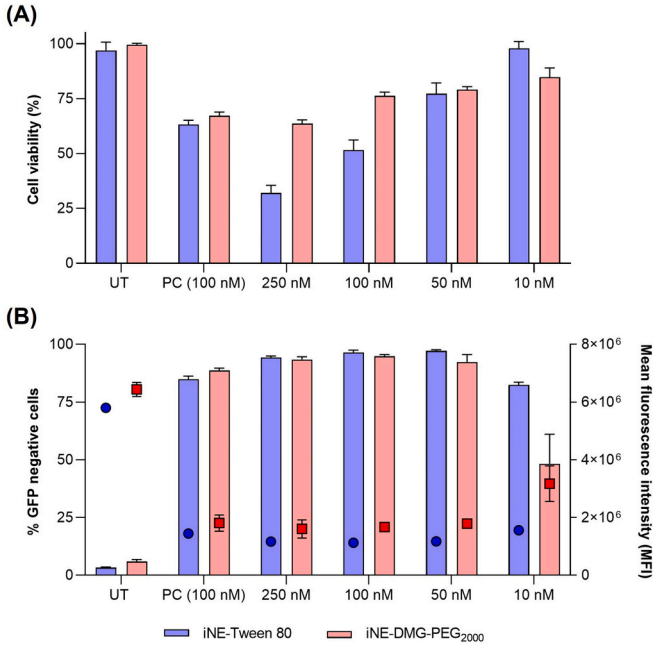

Fig. 2. Cytotoxicity (A) and GFP silencing effect (B) of iNE-Tween 80® (blue) and iNE-DMG-PEG$_{2000}$ (red) containing siGFP, in HeLa cells expressing GFP. The silencing effect was determined in terms of the percentage of GFP negative cells (B, left axis, bars) and mean fluorescence intensity (B, right axis, symbols). (For interpretation of the references to colour in this figure legend, the reader is referred to the web version of this article.)
Abbreviations: DMG-PEG$_{2000}$: (*R*)-methoxy-polyethyleneglycol-2000-carbamoyl-di-O-myristyl-sn-glyceride. GFP: Green fluorescence protein. iNE: Ionizable nanoemulsion. MFI: Mean fluorescence intensity. PC: Positive control, lipofectamine. siGFP: siRNA anti-GFP. UT: Untreated. Values represent the mean ± standard deviation ($n \geq 3$)

3.3. *In vitro evaluation of iNEs in neuron, astrocyte, and microglia cellular models*

To evaluate the ability of iNE nanosystems to deliver oligonucleotides to the brain, *in vitro* studies were conducted using human neurons

(SH-SY5Y), rat astrocytes (C6), and human microglia (CHME-3 cells) cell models, with mGFP as the model nucleic acid (Fig. 3). No toxicity was observed at any of the tested concentrations in the different cell models (Fig. 3-A) when compared to untreated cells.

Regarding the transfection efficiency, significant levels of GFP-transfected cells were detected in all three cellular models, each exhibiting over 70% GFP-positive cells (Fig. 3-B). The slightly higher levels of transfection observed in C6 cells compared to CHME-3 cells could be attributed to greater cellular uptake by astrocytes over microglia cells. On the other hand, regarding the fluorescence intensity values, iNE-mGFP resulted in significantly increased levels for both neurons and microglia models (Fig. 3-C). However, a significantly lower transfection efficiency was observed for astrocytes, where no significant differences were found when compared with the untreated cells. A plausible explanation of this observation could be related to a lower uptake capacity or distinct intracellular trafficking of astrocytes as compared to the neuronal and microglia cells.

3.4. *In vivo evaluation of CNS diffusivity of iNEs encapsulating mGFP*

With the aim of simultaneously evaluating diffusivity and functional performance, iNEs loaded with mGFP were directly administered in the brain, following intra-parenchymal (intrathalamic) injection, in rats. Fig. 4 shows the transfection in neurons, astrocytes, and microglia at 24 h post-administration. Neuron analysis required a double immunolabelling process due to inherent fluorescence in neurons (Supplementary Fig. 1). The images exhibited distinct GFP signals in neurons, indicating the uptake of iNEs by this cell type and the subsequent translation of the reporter protein. Moreover, a specificity of iNEs for neurons *vs* microglia and astrocytes was noted (Fig. 4). In terms of microglia uptake, these findings contrast with our previous *in vitro* fluorescence intensity results (Fig. 3-B,C), indicating a lack of correlation between *in vitro-in vivo* outcomes, typically observed with nanoparticles [51,52]. These results imply the potential of iNEs to effectively evade microglia cells, known as the resident macrophages of the CNS [53,54].

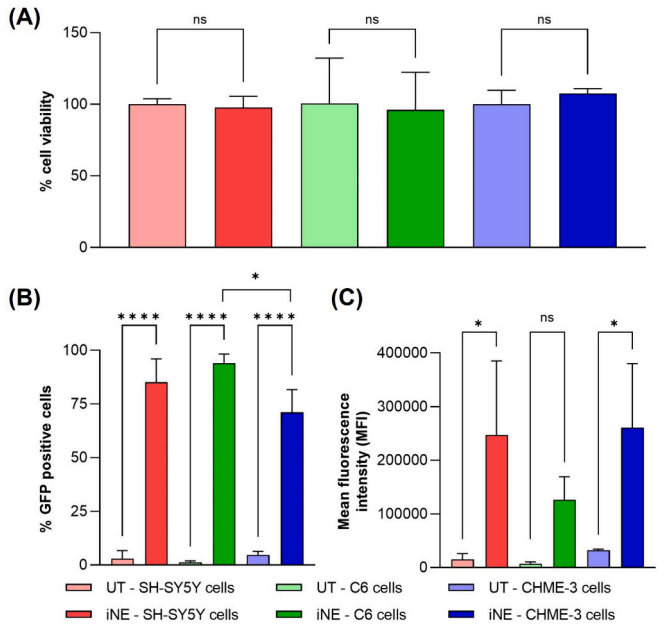

Fig. 3. Cytotoxicity (A) and GFP transfection efficiency (B–C) of iNE-mGFP (bright colour) in a neuron (red), astrocyte (green), and microglia (blue) cellular models. Transfection efficiency was determined in terms of the percentage of GFP-positive cells (B) and mean fluorescence intensity (C). Comparison was made with untreated cells (pale colour). (For interpretation of the references to colour in this figure legend, the reader is referred to the web version of this article.)

Abbreviations: GFP: Green fluorescence protein. iNE: Ionizable nanoemulsion. MFI: Mean fluorescence intensity. mGFP: mRNA encoding GFP. UT: Untreated. A significant comparison was performed using an ordinary one-way ANOVA followed by Tukey's multiple comparison tests between groups. *P*-values < 0.05 were considered statistically significant (*). Also, (****) if *p*-value < 0.0001. Ns: Not significative. Values represent the mean ± standard deviation ($n \geq 3$)

Overall, these results suggest that transfection to specific brain cells could be dependent on the identity of the nanoparticle itself. In agreement with this, classical LNPs efficiently were reported to transfect neurons, astrocytes and, to a minor extent, the microglia cells, upon direct administration in the brain [55]. Good transfection values in neurons and astrocytes were also reported for LNPs containing thiol-cleavable lipids, upon intracerebroventricular (ICV) administration [17]. Of note, microglia cells were not included in this study. As a different delivery approach, other authors have found that polycaprolactone-based nanoparticles could be designed to be directed specifically to microglia cells [56]. Despite these studies, as for now, no clear explanation for the different cellular preferences of different nanoparticles has been identified. We hypothesize that the composition of the nanoparticles influences the resulting protein corona around the nanocarriers, leading to different cellular uptake and even intracellular fate.

The high specificity for neurons underscores the potential of our iNEs for the treatment of brain diseases that could benefit from direct CNS administration, such as glioblastoma or Parkinson's disease [57–60]. However, it is essential to interpret this conclusion cautiously, considering that biodistribution may be significantly different by the influence of these disease conditions.

Following the assessment of the transfection efficiency of iNE, the diffusivity of the nanocarriers throughout the entire brain of the animals was investigated (Fig. 5). Interestingly, a notable diffusion was observed from the injection site, as indicated by a red GFP signal, to more distant areas within the same hemisphere. This observation is remarkable if we consider the limited literature evaluating the diffusion of mRNA-loaded nanoparticles in the brain. In a recent study, traditional LNPs carrying Cre mRNA were directly injected into the striatum and hippocampus of animals. This led to gene editing away from the injection site, with a diffusion range of 1.2–2.7 mm, depending on the site of injection and the dose administered [55]. These results are supported by other mRNA-containing LNPs administered ICV, leading to 1–1.5 mm diffusion patterns from the injection site [15,16]. Our iNE revealed cells expressing GFP up to approximately 3.4 mm apart, based on fluorescent expression on close-up images (Supplementary Fig. 2). This validates our hypothesis that soft fluid cores could enhance the diffusion of nanocarriers. Nevertheless, it is crucial to note that the site and rate of administration may also impact the diffusion pattern of the nanoparticles, and that further diffusion measurements would be needed to better understand the distribution pattern of our iNEs.

Close-up images further confirmed the colocalization of the fluorescence protein in neurons and were used to estimate the diffusion distance of our iNEs (Supplementary Fig. 2). The specificity of the signal was confirmed by the absence of fluorescence upon PBS administration (Supplementary Fig. 3).

Overall, based on the observed distribution profile, we have hypothesized that the diffusion of our iNEs is influenced by the oily core of the iNE nanocarrier. Previous work in our group with polyaminoacid nanocapsules (containing an oily core) showed tissue diffusivity following subcutaneous administration could be enhanced by tunning particle diameter (around 100 nm) and surface nanocarrier composition [34,61]. In this regard, based on previous reports, we could argue that the PEG components of the surface of iNEs could enhance diffusivity [30–32].

These findings underscore the potential of iNEs to diffuse to various brain areas and efficiently transfect mRNA specifically into neurons, further confirming the transduction of the desired model protein. The

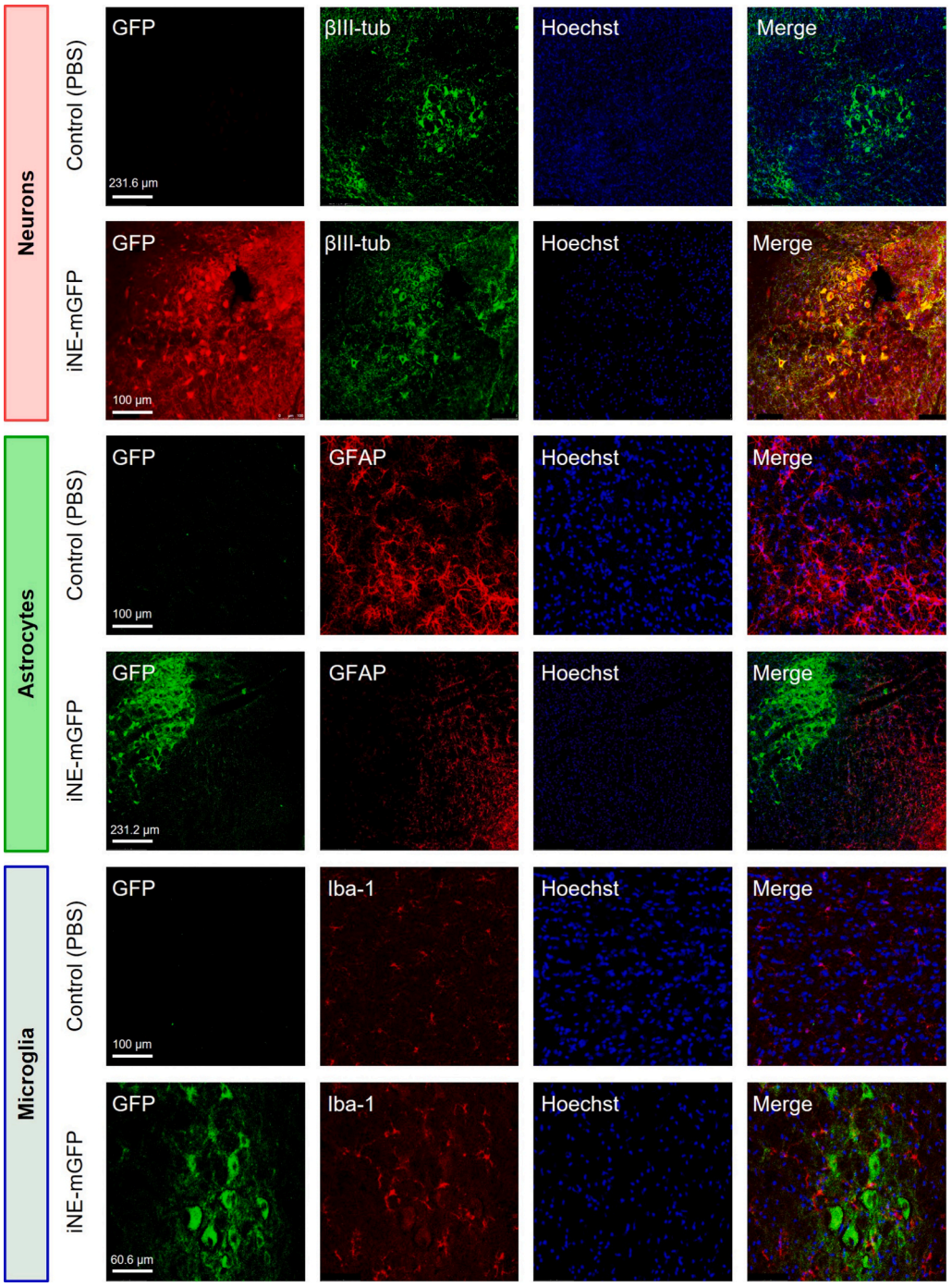

Fig. 4. Immunolabelling for GFP in neurons (labeled with βIII-tubulin), astrocytes (labeled with GFAP), and microglia (labeled with Iba-1) cells in rats after intraparenchymal administration of control (PBS) or iNE-mGFP. Hoechst was used as nuclei marker.
Abbreviations: βIII-tubulin: Class III β-tubulin. GFAP: Glial fibrillary acidic protein. GFP: Green fluorescence protein. Iba-1: Ionized calcium-binding adaptor molecule 1. iNE: Ionizable nanoemulsion. mGFP: mRNA encoding GFP

results suggest that iNE can facilitate the delivery of genetic cargo to different brain regions following a single administration.

4. Conclusions

Here, a new RNA delivery carrier named iNE, exhibiting a unique profile as compared to the classical LNPs, is disclosed. The iNEs exhibited sub-100 nm size, neutral surface charge, high RNA entrapment capacity, and favorable transfection profile in different cell lines *in vitro*, notably in neuronal and microglia cells. While these properties may be common to other nanocarriers, iNEs showed an advantageous profile marked by their high diffusivity across the brain tissue upon their direct administration in rat parenchyma.

In summary, this research outlines the development of a novel class of ionizable nanocarriers tailored for RNA delivery to the brain, showcasing a promising diffusion pattern and specific targeting capabilities for neurons. These nanocarriers hold significant promise for addressing diverse CNS diseases, including glioblastoma or Parkinson's disease.

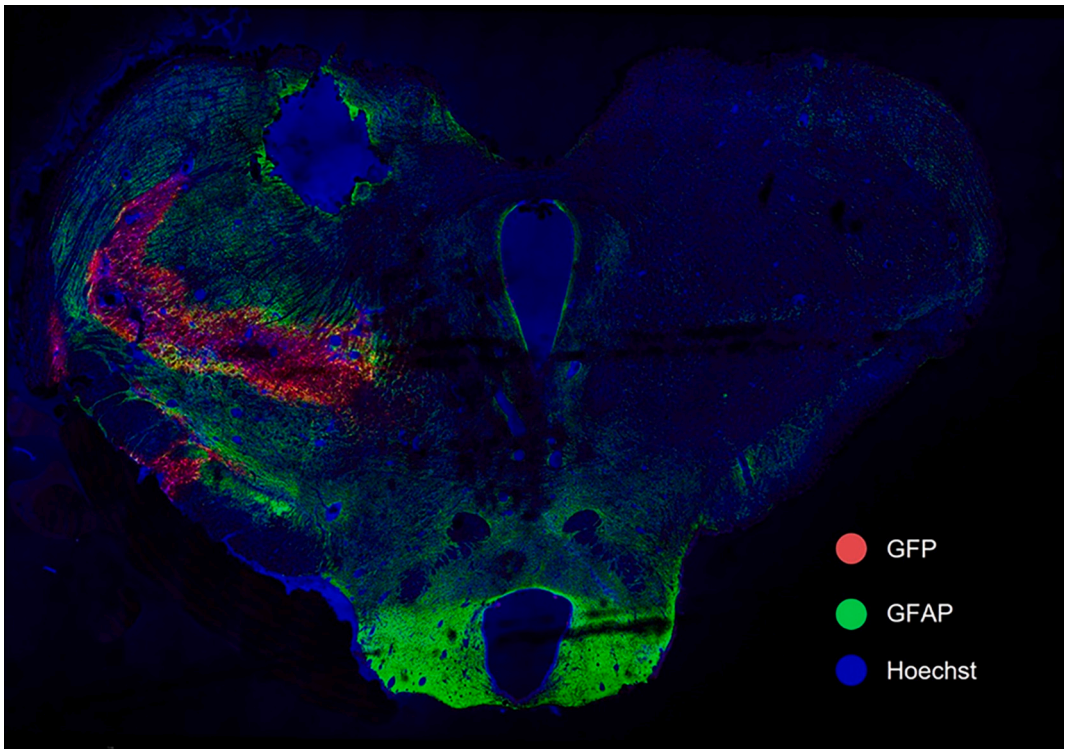

Fig. 5. Double immunolabelling in the whole brain for GFP (red) and astrocytes (labeled with GFAP, green), after intraparenchymal administration of iNE-mGFP. Hoechst was used as nuclei marker (blue). (For interpretation of the references to colour in this figure legend, the reader is referred to the web version of this article.) Abbreviations: GFAP: Glial fibrillary acidic protein. GFP: Green fluorescence protein. iNE: Ionizable nanoemulsion. mGFP: mRNA encoding GFP

CRediT authorship contribution statement

Mireya L. Borrajo: Conceptualization, Data curation, Formal analysis, Investigation, Methodology, Validation, Writing – original draft, Writing – review & editing, Visualization. **Aloia Quijano:** Formal analysis, Investigation, Methodology, Validation, Visualization. **Philipp Lapuhs:** Formal analysis, Investigation, Methodology, Validation, Writing – review & editing. **Ana I. Rodriguez-Perez:** Investigation, Methodology, Validation. **Shubaash Anthiya:** Conceptualization, Investigation, Methodology, Writing – review & editing. **José L. Labandeira-Garcia:** Conceptualization, Funding acquisition, Resources, Supervision, Writing – review & editing. **Rita Valenzuela:** Conceptualization, Data curation, Formal analysis, Investigation, Methodology, Project administration, Supervision, Validation, Visualization, Writing – original draft, Writing – review & editing. **María José Alonso:** Conceptualization, Data curation, Funding acquisition, Project administration, Resources, Supervision, Writing – original draft, Writing – review & editing.

Data availability

Data will be made available on request.

Acknowledgments

This work was supported by B-SMART project, funded by the European Union's Horizon 2020 research and innovation program under grant agreement No 721058. Authors also acknowledge the Competitive Reference Groups, Consellería de Educación e Ordenación Universitaria, Xunta de Galicia (Ref. ED431C 2021/17 and ED431C 22/41). Financial support from the Xunta de Galicia (Centro singular de Investigación de Galicia accreditation 2019-2022), the (European Union European Regional Development Fund – ERDF), and the Spanish Ministry of Science and Innovation (PID2021-126848NB-100) are gratefully acknowledged. Mireya L. Borrajo acknowledges the financial support by Instituto de Salud Carlos III through the "Contratos i-PFIS: Doctorados ISS-empresa en Ciencias y Tecnologías de la Salud" (IFI19/00033). The authors also want to acknowledge Muthiah Manoharan, from Alnylam Pharmaceuticals (MA, USA) for generously providing C12-200 and DMG-PEG$_{2000}$ lipids for our experiments. Graphical abstract was created with BioRender.com.

Appendix A. Supplementary data

Supplementary data to this article can be found online at https://doi.org/10.1016/j.jconrel.2024.06.051.

References

[1] M. Verma, I. Ozer, W. Xie, R. Gallagher, A. Teixeira, M. Choy, The landscape for lipid-nanoparticle-based genomic medicines, Nat. Rev. Drug Discov. 22 (2023) 349–350, https://doi.org/10.1038/d41573-023-00002-2.
[2] S.M. Hoy, Patisiran: first global approval, Drugs 78 (2018) 1625–1631, https://doi.org/10.1007/s40265-018-0983-6.
[3] T. Fiolet, Y. Kherabi, C.-J. MacDonald, J. Ghosn, N. Peiffer-Smadja, Comparing COVID-19 vaccines for their characteristics, efficacy and effectiveness against SARS-CoV-2 and variants of concern: a narrative review, Clin. Microbiol. Infect. 28 (2022) 202–221, https://doi.org/10.1016/j.cmi.2021.10.005.
[4] J. Kim, Y. Eygeris, M. Gupta, G. Sahay, Self-assembled mRNA vaccines, Adv. Drug Deliv. Rev. 170 (2021) 83–112, https://doi.org/10.1016/j.addr.2020.12.014.
[5] P.R. Cullis, M.J. Hope, Lipid nanoparticle Systems for Enabling Gene Therapies, Mol. Ther. 25 (2017) 1467–1475, https://doi.org/10.1016/j.ymthe.2017.03.013.
[6] G. Sahay, D.Y. Alakhova, A.V. Kabanov, Endocytosis of nanomedicines, J. Control. Release 145 (2010) 182–195, https://doi.org/10.1016/j.jconrel.2010.01.036.
[7] S. Patel, J. Kim, M. Herrera, A. Mukherjee, A.V. Kabanov, G. Sahay, Brief update on endocytosis of nanomedicines, Adv. Drug Deliv. Rev. 144 (2019) 90–111, https://doi.org/10.1016/j.addr.2019.08.004.
[8] J. Heyes, L. Palmer, K. Bremner, I. MacLachlan, Cationic lipid saturation influences intracellular delivery of encapsulated nucleic acids, J. Control. Release 107 (2005) 276–287, https://doi.org/10.1016/j.jconrel.2005.06.014.
[9] M. Jayaraman, S.M. Ansell, B.L. Mui, Y.K. Tam, J. Chen, X. Du, D. Butler, L. Eltepu, S. Matsuda, J.K. Narayanannair, K.G. Rajeev, I.M. Hafez, A. Akinc, M.A. Maier, M. A. Tracy, P.R. Cullis, T.D. Madden, M. Manoharan, M.J. Hope, Maximizing the

potency of siRNA lipid nanoparticles for hepatic gene silencing in vivo, Angew. Chemie Int. Ed. 51 (2012) 8529–8533, https://doi.org/10.1002/anie.201203263.
[10] X. Han, H. Zhang, K. Butowska, K.L. Swingle, M.G. Alameh, D. Weissman, M. J. Mitchell, An ionizable lipid toolbox for RNA delivery, Nat. Commun. 12 (2021) 8–13, https://doi.org/10.1038/s41467-021-27493-0.
[11] A.M. Reichmuth, M.A. Oberli, A. Jaklenec, R. Langer, D. Blankschtein, mRNA vaccine delivery using lipid nanoparticles, Ther. Deliv. 7 (2016) 319–334, https://doi.org/10.4155/tde-2016-0006.
[12] A.M. Jörgensen, R. Wibel, A. Bernkop-Schnürch, Biodegradable cationic and ionizable cationic lipids: a roadmap for safer pharmaceutical excipients, Small 19 (2023), https://doi.org/10.1002/smll.202206968.
[13] Z. Chen, Y. Tian, J. Yang, F. Wu, S. Liu, W. Cao, W. Xu, T. Hu, D.J. Siegwart, H. Xiong, Modular design of biodegradable ionizable lipids for improved mrna delivery and precise cancer metastasis delineation in vivo, J. Am. Chem. Soc. 145 (2023) 24302–24314, https://doi.org/10.1021/jacs.3c09143.
[14] L. Xue, A.G. Hamilton, G. Zhao, Z. Xiao, R. El-Mayta, X. Han, N. Gong, X. Xiong, J. Xu, C.G. Figueroa-Espada, S.J. Shepherd, A.J. Mukalel, M.-G. Alameh, J. Cui, K. Wang, A.E. Vaughan, D. Weissman, M.J. Mitchell, High-throughput barcoding of nanoparticles identifies cationic, degradable lipid-like materials for mRNA delivery to the lungs in female preclinical models, Nat. Commun. 15 (2024) 1884, https://doi.org/10.1038/s41467-024-45422-9.
[15] R.L. Rungta, H.B. Choi, P.J. Lin, R.W. Ko, D. Ashby, J. Nair, M. Manoharan, P. R. Cullis, B.A. MacVicar, Lipid nanoparticle delivery of siRNA to silence neuronal gene expression in the brain, Mol. Ther. Acids. 2 (2013) e136, https://doi.org/10.1038/mtna.2013.65.
[16] L.E. Waggoner, K.F. Miyasaki, E.J. Kwon, Analysis of PEG-lipid anchor length on lipid nanoparticle pharmacokinetics and activity in a mouse model of traumatic brain injury, Biomater. Sci. (2023) 4238–4253, https://doi.org/10.1039/d2bm01846b.
[17] H. Tanaka, T. Nakatani, T. Furihata, K. Tange, Y. Nakai, H. Yoshioka, H. Harashima, H. Akita, In vivo introduction of mRNA encapsulated in lipid nanoparticles to brain neuronal cells and astrocytes via Intracerebroventricular administration, Mol. Pharm. 15 (2018) 2060–2067, https://doi.org/10.1021/acs.molpharmaceut.7b01084.
[18] S. Liu, J. Liu, H. Li, K. Mao, H. Wang, X. Meng, J. Wang, C. Wu, H. Chen, X. Wang, X. Cong, Y. Hou, Y. Wang, M. Wang, Y.-G. Yang, T. Sun, An optimized ionizable cationic lipid for brain tumor-targeted siRNA delivery and glioblastoma immunotherapy, Biomaterials 287 (2022) 121645, https://doi.org/10.1016/j.biomaterials.2022.121645.
[19] Y. Eygeris, S. Patel, A. Jozic, G. Sahay, Deconvoluting lipid nanoparticle structure for messenger RNA delivery, Nano Lett. 20 (2020) 4543–4549, https://doi.org/10.1021/acs.nanolett.0c01386.
[20] A.B. Etame, R.J. Diaz, M.A. O'Reilly, C.A. Smith, T.G. Mainprize, K. Hynynen, J. T. Rutka, Enhanced delivery of gold nanoparticles with therapeutic potential into the brain using MRI-guided focused ultrasound, nanomedicine nanotechnology, Biol. Med. 8 (2012) 1133–1142, https://doi.org/10.1016/j.nano.2012.02.003.
[21] S. Pan, P.H. Yang, D. DeFreitas, S. Ramagiri, P.O. Bayguinov, C.D. Hacker, A. Z. Snyder, J. Wilborn, H. Huang, G.M. Koller, D.K. Raval, G.L. Halupnik, S. Sviben, S. Achilefu, R. Tang, G. Haller, J.D. Quirk, J.A.J. Fitzpatrick, P. Esakky, J. M. Strahle, Gold nanoparticle-enhanced X-ray microtomography of the rodent reveals region-specific cerebrospinal fluid circulation in the brain, Nat. Commun. 14 (2023) 453, https://doi.org/10.1038/s41467-023-36083-1.
[22] A.A. Date, N. Desai, R. Dixit, M. Nagarsenker, Self-nanoemulsifying drug delivery systems: formulation insights, applications and advances, Nanomedicine 5 (2010) 1595–1616, https://doi.org/10.2217/nnm.10.126.
[23] M.R. Patel, R.B. Patel, S.D. Thakore, Nanoemulsion in drug delivery, in: Appl. Nanocomposite Mater. Drug Deliv, Elsevier, 2018, pp. 667–700, https://doi.org/10.1016/B978-0-12-813741-3.00030-3.
[24] K.B. Sutradhar, M.L. Amin, Nanoemulsions: increasing possibilities in drug delivery, Eur. J. Nanomedicine. 5 (2013), https://doi.org/10.1515/ejnm-2013-0001.
[25] L.A. Brito, M. Chan, C.A. Shaw, A. Hekele, T. Carsillo, M. Schaefer, J. Archer, A. Seubert, G.R. Otten, C.W. Beard, A.K. Dey, A. Lilja, N.M. Valiante, P.W. Mason, C.W. Mandl, S.W. Barnett, P.R. Dormitzer, J.B. Ulmer, M. Singh, D.T. O'Hagan, A. J. Geall, A cationic nanoemulsion for the delivery of next-generation RNA vaccines, Mol. Ther. 22 (2014) 2118–2129, https://doi.org/10.1038/mt.2014.133.
[26] W.M. Bogers, H. Oostermeijer, P. Mooij, G. Koopman, E.J. Verschoor, D. Davis, J. B. Ulmer, L.A. Brito, Y. Cu, K. Banerjee, G.R. Otten, B. Burke, A. Dey, J.L. Heeney, X. Shen, G.D. Tomaras, C. Labranche, D.C. Montefiori, H.-X. Liao, B. Haynes, A. J. Geall, S.W. Barnett, Potent immune responses in Rhesus macaques induced by nonviral delivery of a self-amplifying RNA vaccine expressing HIV type 1 envelope with a cationic nanoemulsion, J Infect Dis 211 (2015) 947–955, https://doi.org/10.1093/infdis/jiu522.
[27] P.T. Wong, P.H. Goff, R.J. Sun, M.J. Ruge, M.E. Ermler, A. Sebring, J.J. O'Konek, J. J. Landers, K.W. Janczak, W. Sun, J.R. Baker, Combined intranasal Nanoemulsion and RIG-I activating RNA adjuvants enhance mucosal, humoral, and cellular immunity to influenza virus, Mol. Pharm. 18 (2021) 679–698, https://doi.org/10.1021/acs.molpharmaceut.0c00315.
[28] S. Yadav, S.K. Gandham, R. Panicucci, M.M. Amiji, Intranasal brain delivery of cationic nanoemulsion-encapsulated TNFα siRNA in prevention of experimental neuroinflammation, Elsevier Inc. (2016), https://doi.org/10.1016/j.nano.2015.12.374.
[29] J.H. Azambuja, R.S. Schuh, L.R. Michels, N.E. Gelsleichter, L.R. Beckenkamp, I. C. Iser, G.S. Lenz, F.H. de Oliveira, G. Venturin, S. Greggio, J.C. DaCosta, M. R. Wink, J. Sevigny, M.A. Stefani, A.M.O. Battastini, H.F. Teixeira, E. Braganhol, Nasal administration of cationic nanoemulsions as CD73-siRNA delivery system for glioblastoma treatment: a new therapeutical approach, Mol. Neurobiol. 57 (2020) 635–649, https://doi.org/10.1007/s12035-019-01730-6.
[30] S.K. Lai, D.E. O'Hanlon, S. Harrold, S.T. Man, Y.-Y. Wang, R. Cone, J. Hanes, Rapid transport of large polymeric nanoparticles in fresh undiluted human mucus, Proc. Natl. Acad. Sci. 104 (2007) 1482–1487, https://doi.org/10.1073/pnas.0608611104.
[31] E.A. Nance, G.F. Woodworth, K.A. Sailor, T.-Y. Shih, Q. Xu, G. Swaminathan, D. Xiang, C. Eberhart, J. Hanes, A dense poly(ethylene glycol) coating improves penetration of large polymeric nanoparticles within brain tissue, Sci. Transl. Med. 4 (2012) 1–7, https://doi.org/10.1126/scitranslmed.3003594.
[32] D. Rao, G. Kwak, H. Wang, C.G. Eberhart, J. Hanes, J.S. Suk, Bioreducible gene delivery platform that promotes intracellular payload release and widespread brain dispersion, ACS Biomater Sci. Eng. 9 (2023) 4567–4572, https://doi.org/10.1021/acsbiomaterials.3c00799.
[33] M. Peleteiro, E. Presas, J.V. González-Aramundiz, B. Sánchez-Correa, R. Simón-Vázquez, N. Csaba, M.J. Alonso, Á. González-Fernández, Polymeric nanocapsules for vaccine delivery: influence of the polymeric shell on the interaction with the immune system, Front. Immunol. 9 (2018), https://doi.org/10.3389/fimmu.2018.00791.
[34] R. Abellan-Pose, C. Teijeiro-Valiño, M.J. Santander-Ortega, E. Borrajo, A. Vidal, M. Garcia-Fuentes, N. Csaba, M.J. Alonso, Polyaminoacid nanocapsules for drug delivery to the lymphatic system: effect of the particle size, Int. J. Pharm. 509 (2016) 107–117, https://doi.org/10.1016/j.ijpharm.2016.05.034.
[35] J.V. González-Aramundiz, E. Presas, I. Dalmau-Mena, S. Martínez-Pulgarín, C. Alonso, J.M. Escribano, M.J. Alonso, N.S. Csaba, Rational design of protamine nanocapsules as antigen delivery carriers, J. Control. Release 245 (2017) 62–69, https://doi.org/10.1016/j.jconrel.2016.11.012.
[36] A.S. Cordeiro, J. Crecente-Campo, B.L. Bouzo, S.F. González, M. de la Fuente, M. J. Alonso, Engineering polymeric nanocapsules for an efficient drainage and biodistribution in the lymphatic system, J. Drug Target. 27 (2019) 646–658, https://doi.org/10.1080/1061186X.2018.1561886.
[37] J. Crecente-Campo, M.J. Alonso, Engineering, on-demand manufacturing, and scaling-up of polymeric nanocapsules, Bioeng. Transl. Med. 4 (2019) 38–50, https://doi.org/10.1002/btm2.10118.
[38] J. Crecente-Campo, S. Lorenzo-Abalde, A. Mora, J. Marzoa, N. Csaba, J. Blanco, Á. González-Fernández, M.J. Alonso, Bilayer polymeric nanocapsules: a formulation approach for a thermostable and adjuvanted E. Coli antigen vaccine, J. Control. Release 286 (2018) 20–32, https://doi.org/10.1016/j.jconrel.2018.07.018.
[39] G. Berrecoso, J. Crecente-Campo, M.J. Alonso, Quantification of the actual composition of polymeric nanocapsules: a quality control analysis, Drug Deliv. Transl. Res. 12 (2022) 2865–2874, https://doi.org/10.1007/s13346-022-01150-5.
[40] P. Calvo, C. Remuñán-López, J.L. Vila-Jato, M.J. Alonso, Development of positively charged colloidal drug carriers: chitosan-coated polyester nanocapsules and submicron-emulsions, Colloid Polym. Sci. 275 (1997) 46–53, https://doi.org/10.1007/s003960050050.
[41] D.P. Ivanov, A.M. Grabowska, M.C. Garnett, High-throughput spheroid screens using volume, resazurin reduction, and acid phosphatase activity, Methods Mol. Biol. 1601 (2017) 43–59, https://doi.org/10.1007/978-1-4939-6960-9_4.
[42] N. Spitzer, G.S. Sammons, E.M. Price, Autofluorescent cells in rat brain can be convincing impostors in green fluorescent reporter studies, J. Neurosci. Methods 197 (2011) 48–55, https://doi.org/10.1016/j.jneumeth.2011.01.029.
[43] A.K. Blakney, P.F. McKay, B.I. Yus, Y. Aldon, R.J. Shattock, Inside out: optimization of lipid nanoparticle formulations for exterior complexation and in vivo delivery of saRNA, Gene Ther. 26 (2019) 363–372, https://doi.org/10.1038/s41434-019-0095-2.
[44] S.C. Semple, A. Akinc, J. Chen, A.P. Sandhu, B.L. Mui, C.K. Cho, D.W.Y. Sah, D. Stebbing, E.J. Crosley, E. Yaworski, I.M. Hafez, J.R. Dorkin, J. Qin, K. Lam, K. G. Rajeev, K.F. Wong, L.B. Jeffs, L. Nechev, M.L. Eisenhardt, M. Jayaraman, M. Kazem, M.A. Maier, M. Srinivasulu, M.J. Weinstein, Q. Chen, R. Alvarez, S. A. Barros, S. De, S.K. Klimuk, T. Borland, V. Kosovrasti, W.L. Cantley, Y.K. Tam, M. Manoharan, M.A. Ciufolini, M.A. Tracy, A. De Fougerolles, I. MacLachlan, P. R. Cullis, T.D. Madden, M.J. Hope, Rational design of cationic lipids for siRNA delivery, Nat. Biotechnol. 28 (2010) 172–176, https://doi.org/10.1038/nbt.1602.
[45] N.M. Belliveau, J. Huft, P.J. Lin, S. Chen, A.K. Leung, T.J. Leaver, A.W. Wild, J. B. Lee, R.J. Taylor, Y.K. Tam, C.L. Hansen, P.R. Cullis, Microfluidic synthesis of highly potent limit-size lipid nanoparticles for in vivo delivery of siRNA, Mol. Ther. - Nucleic Acids. 1 (2012) e37, https://doi.org/10.1038/mtna.2012.28.
[46] K. Okuda, Y. Sato, K. Iwakawa, K. Sasaki, N. Okabe, M. Maeki, M. Tokeshi, H. Harashima, On the size-regulation of RNA-loaded lipid nanoparticles synthesized by microfluidic device, J. Control. Release 348 (2022) 648–659, https://doi.org/10.1016/j.jconrel.2022.06.017.
[47] A. Sarode, Y. Fan, A.E. Byrnes, M. Hammel, G.L. Hura, Y. Fu, P. Kou, C. Hu, F. I. Hinz, J. Roberts, S.G. Koenig, K. Nagapudi, C.C. Hoogenraad, T. Chen, D. Leung, C.-W. Yen, Predictive high-throughput screening of PEGylated lipids in oligonucleotide-loaded lipid nanoparticles for neuronal gene silencing, Nanoscale Adv. 4 (2022) 2107–2123, https://doi.org/10.1039/D1NA00712B.
[48] L.M. Bareford, P.W. Swaan, Endocytic mechanisms for targeted drug delivery, Adv. Drug Deliv. Rev. 59 (2007) 748–758, https://doi.org/10.1016/j.addr.2007.06.008.
[49] J.R. Casey, S. Grinstein, J. Orlowski, Sensors and regulators of intracellular pH, Nat. Rev. Mol. Cell Biol. 11 (2010) 50–61, https://doi.org/10.1038/nrm2820.
[50] I. Canton, G. Battaglia, Endocytosis at the nanoscale, Chem. Soc. Rev. 41 (2012) 2718, https://doi.org/10.1039/c2cs15309b.
[51] K. Paunovska, C.D. Sago, C.M. Monaco, W.H. Hudson, M.G. Castro, T.G. Rudoltz, S. Kalathoor, D.A. Vanover, P.J. Santangelo, R. Ahmed, A.V. Bryksin, J.E. Dahlman, A direct comparison of in vitro and in vivo nucleic acid delivery mediated by

hundreds of nanoparticles reveals a weak correlation, Nano Lett. 18 (2018) 2148–2157, https://doi.org/10.1021/acs.nanolett.8b00432.
[52] T.G. Agnihotri, A. Alexander, M. Agrawal, S.K. Dubey, A. Jain, In vitro-in vivo correlation in nanocarriers: from protein corona to therapeutic implications, J. Control. Release 354 (2023) 794–809, https://doi.org/10.1016/j.jconrel.2023.01.063.
[53] Q. Li, B.A. Barres, Microglia and macrophages in brain homeostasis and disease, Nat. Rev. Immunol. 18 (2018) 225–242, https://doi.org/10.1038/nri.2017.125.
[54] C. García-Cáceres, E. Balland, V. Prevot, S. Luquet, S.C. Woods, M. Koch, T. L. Horvath, C.-X. Yi, J.A. Chowen, A. Verkhratsky, A. Araque, I. Bechmann, M. H. Tschöp, Role of astrocytes, microglia, and tanycytes in brain control of systemic metabolism, Nat. Neurosci. 22 (2019) 7–14, https://doi.org/10.1038/s41593-018-0286-y.
[55] J. Tuma, Y.-J. Chen, M.G. Collins, A. Paul, J. Li, H. Han, R. Sharma, N. Murthy, H. Y. Lee, Lipid nanoparticles deliver mRNA to the brain after an intracerebral injection, Biochemistry 62 (2023) 3533–3547, https://doi.org/10.1021/acs.biochem.3c00371.
[56] M. Peviani, U. Capasso Palmiero, F. Cecere, R. Milazzo, D. Moscatelli, A. Biffi, Biodegradable polymeric nanoparticles administered in the cerebrospinal fluid: brain biodistribution, preferential internalization in microglia and implications for cell-selective drug release, Biomaterials 209 (2019) 25–40, https://doi.org/10.1016/j.biomaterials.2019.04.012.
[57] C. Marogianni, M. Sokratous, E. Dardiotis, G.M. Hadjigeorgiou, D. Bogdanos, G. Xiromerisiou, Neurodegeneration and inflammation—an interesting interplay in Parkinson's disease, Int. J. Mol. Sci. 21 (2020) 8421, https://doi.org/10.3390/ijms21228421.
[58] X.-Y. Chen, C. Liu, Y. Xue, L. Chen, Changed firing activity of nigra dopaminergic neurons in Parkinson's disease, Neurochem. Int. 162 (2023) 105465, https://doi.org/10.1016/j.neuint.2022.105465.
[59] V. Venkataramani, Y. Yang, M.C. Schubert, E. Reyhan, S.K. Tetzlaff, N. Wißmann, M. Botz, S.J. Soyka, C.A. Beretta, R.L. Pramatarov, L. Fankhauser, L. Garofano, A. Freudenberg, J. Wagner, D.I. Tanev, M. Ratliff, R. Xie, T. Kessler, D. C. Hoffmann, L. Hai, Y. Dörflinger, S. Hoppe, Y.A. Yabo, A. Golebiewska, S. P. Niclou, F. Sahm, A. Lasorella, M. Slowik, L. Döring, A. Iavarone, W. Wick, T. Kuner, F. Winkler, Glioblastoma hijacks neuronal mechanisms for brain invasion, Cell 185 (2022), https://doi.org/10.1016/j.cell.2022.06.054, 2899–2917.e31.
[60] S. Krishna, A. Choudhury, M.B. Keough, K. Seo, L. Ni, S. Kakaizada, A. Lee, A. Aabedi, G. Popova, B. Lipkin, C. Cao, C. Nava Gonzales, R. Sudharshan, A. Egladyous, N. Almeida, Y. Zhang, A.M. Molinaro, H.S. Venkatesh, A.G.S. Daniel, K. Shamardani, J. Hyer, E.F. Chang, A. Findlay, J.J. Phillips, S. Nagarajan, D. R. Raleigh, D. Brang, M. Monje, S.L. Hervey-Jumper, Glioblastoma remodelling of human neural circuits decreases survival, Nature 617 (2023) 599–607, https://doi.org/10.1038/s41586-023-06036-1.
[61] R. Abellan-Pose, M. Rodríguez-Évora, S. Vicente, N. Csaba, C. Évora, M.J. Alonso, A. Delgado, Biodistribution of radiolabeled polyglutamic acid and PEG-polyglutamic acid nanocapsules, Eur. J. Pharm. Biopharm. 112 (2017) 155–163, https://doi.org/10.1016/j.ejpb.2016.11.015.